Collision cross sections for the thermalization of cold gases

Matthew D. Frye and Jeremy M. Hutson
Joint Quantum Centre (JQC) Durham/Newcastle, Department of Chemistry, Durham University, South Road, Durham DH1 3LE, United Kingdom
(Received 5 March 2014; published 12 May 2014)

The collision cross section that controls thermalization of gas mixtures is the transport cross section $\sigma_\eta^{(1)}$ and not the elastic cross section $\sigma_{\rm el}$. The two are the same for pure s-wave scattering but not when higher partial waves contribute. We investigate the differences between them for prototype atomic mixtures and show that the distinction is important at energies above 100 μK for LiYb and 3 μK for RbYb and RbCs. For simple systems, both $\sigma_\eta^{(1)}$ and $\sigma_{\rm el}$ follow universal energy dependence that depends only on the s-wave scattering length when expressed in reduced length and energy units.

DOI: 10.1103/PhysRevA.89.052705 PACS number(s): 34.50.Cx

I. INTRODUCTION

The scattering length for interaction between a pair of atoms or molecules is a key quantity in ultracold physics. It determines the cross sections for ultracold collisions and the energy of a Bose-Einstein condensate. Manipulating the scattering length with applied magnetic, electric, or optical fields provides the main way to control ultracold gases, allowing the investigation of condensate collapse, solitons, molecule formation, and many other phenomena.

Precise determinations of scattering lengths may be achieved by fitting the energies of high-lying bound states or the positions of zero-energy Feshbach resonances as a function of applied field. However, in the early stages of investigating a new ultracold mixture, approximate scattering lengths are often obtained from experimental studies of interspecies thermalization rates, which, in turn, depend on collision cross sections.

It is often supposed that the rate of thermalization is determined by the elastic cross section $\sigma_{\rm el}$ [1–3], which is related to the differential cross section $d\sigma/d\omega$ by

$$\sigma_{\rm el} = \int \frac{d\sigma}{d\omega} d\omega = \int \frac{d\sigma}{d\omega} \sin\,\Theta\, d\Theta, \qquad (1)$$

where Θ is the deflection angle in the center-of-mass frame. However, collisions that cause only small deflections of the collision partners contribute fully to the elastic cross section but make very little contribution to kinetic-energy transfer and thus to thermalization. The appropriate cross section that takes this into account is the transport cross section $\sigma_\eta^{(1)}$,

$$\sigma_\eta^{(1)} = \int \frac{d\sigma}{d\omega}(1-\cos\,\Theta)\sin\,\Theta\, d\Theta, \qquad (2)$$

which has been used extensively in the context of transport properties at higher temperatures [4,5]. It determines the binary diffusion coefficient for a mixture and contributes to the shear viscosity coefficient.

The relevance of $\sigma_\eta^{(1)}$ to thermalization of ultracold gases has been pointed out by Anderlini and Guéry-Odelin [6] (who call it $\widetilde{\sigma}$), but no study of its behavior has been made for the conditions relevant to thermalization of ultracold atoms and molecules. The purpose of the present paper is to explore the behavior of $\sigma_\eta^{(1)}$ and to compare it with $\sigma_{\rm el}$ for cold and ultracold collisions. For this purpose, we will consider two topical systems, LiYb and RbYb, for both of which there have been recent studies of thermalization aimed at determining scattering lengths [7–10]. $\sigma_{\rm el}$ and $\sigma_\eta^{(1)}$ are equivalent when $d\sigma/d\omega$ is isotropic, which is true both for classical hard-sphere collisions and for quantum scattering at limitingly low energy (in the s-wave regime). However, we will show that there are significant differences between $\sigma_{\rm el}$ and $\sigma_\eta^{(1)}$ for realistic potentials and that these should be taken into account when using thermalization results to estimate scattering lengths, particularly in the energy regime where s-wave and p-wave collisions make comparable contributions. In addition, we will show that, for systems of this type, the scattering properties of low-L partial waves with $L > 0$ are almost universal functions of the s-wave scattering length $a_{\rm s}$ and that the behavior of both $\sigma_{\rm el}$ and $\sigma_\eta^{(1)}$ in the few-partial-wave regime can be predicted from knowledge of $a_{\rm s}$ alone.

Expansion of the differential cross section allows an alternative expression for $\sigma_\eta^{(1)}$ to be written in terms of partial-wave phase shifts δ_L [6],

$$\sigma_\eta^{(1)} = \frac{2\pi}{k^2} \sum_{0\leqslant L\leqslant L'<\infty} \alpha_{L,L'} \sin\,\delta_L \sin\,\delta_{L'} \cos(\delta_L - \delta_{L'}), \qquad (3)$$

where $E = \hbar^2 k^2/2\mu$ is the collision energy, μ is the reduced mass, and

$$\alpha_{L,L'} = (2-\delta_{L,L'})(2L+1)(2L'+1)\int_{-1}^{1}(1-x)P_L(x)P_{L'}(x),$$

which evaluates to $\alpha_{L,L} = 4L+2$, $\alpha_{L,L+1} = -(4L+4)$, $\alpha = 0$ otherwise. The equivalent expression for $\sigma_{\rm el}$ contains only the terms with $L = L'$, so the difference between the two cross sections takes the form of a set of interference terms between partial waves with $\Delta L = \pm 1$, which may be either positive or negative.

II. NUMERICAL RESULTS

Systems such as LiYb and RbYb, made up of an alkali-metal atom (^{2}S) and a closed-shell atom (^{1}S), exhibit very narrow Feshbach resonances due to coupling between the alkali-metal hyperfine states due to the dependence of the hyperfine coupling on the internuclear distance R [11–13]. However, these resonances have magnetic-field widths of 100 mG or less; collisions far from resonance can accurately

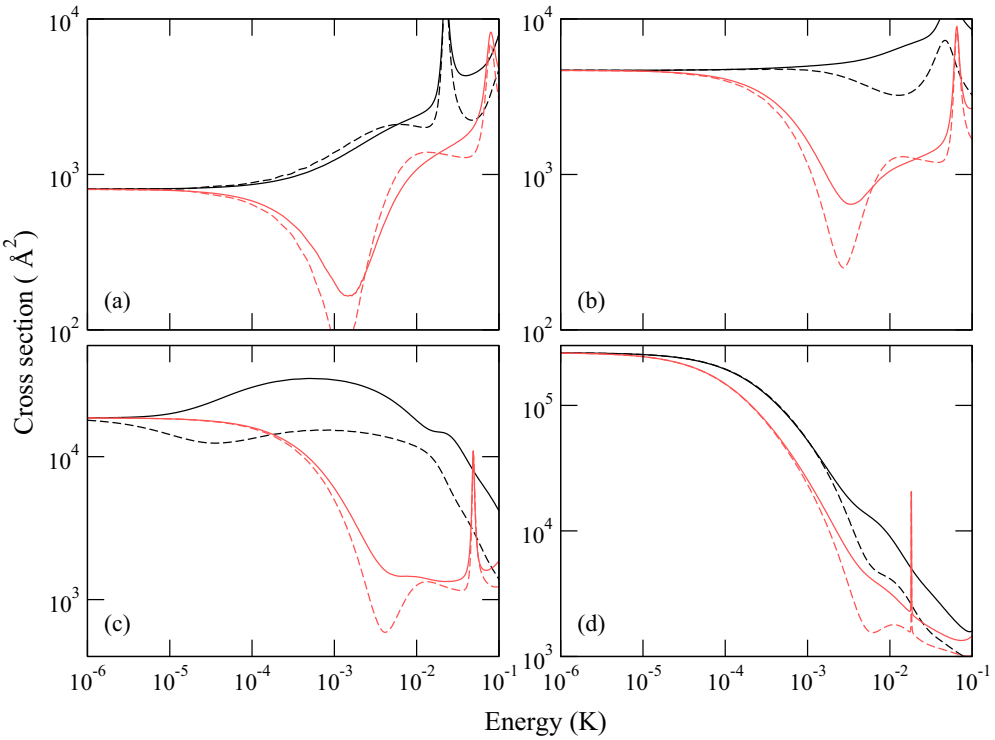

FIG. 1. (Color online) LiYb cross sections. $\sigma_{\rm el}$ (solid lines) and $\sigma_\eta^{(1)}$ (dashed lines) for positive (black) and negative (red, gray) signs of the scattering length for different values of the magnitude of the scattering length: (a) $|a_{\rm s}| = 8$ Å, (b) $|a_{\rm s}| = \bar{a} = 19.3$ Å, (c) $|a_{\rm s}| = 2\bar{a} = 38.6$ Å, and (d) $|a_{\rm s}| = 7.5\bar{a} = 145$ Å.

be described by single-channel calculations that neglect both electron and nuclear spins and are independent of the magnetic field. In the present paper, we solve the single-channel Schrödinger equation using the MOLSCAT package [14]. The SBE postprocessor [15] is then used to calculate $\sigma_\eta^{(1)}$ from S-matrix elements as described by Liu *et al.* [5]. We use interaction potentials for LiYb [16] and RbYb [13] from electronic structure calculations with a fixed long-range C_6 coefficient and the short-range potential scaled by a factor λ to adjust the s-wave scattering lengths as required.

For ^{6}Li^{174}Yb, recent thermalization experiments suggest an s-wave scattering length of $|a_{\rm s}| \approx 8$ Å [7,8], but cannot determine the sign in the low-temperature regime investigated, where only s-wave scattering contributes. However, the sign could be determined from thermalization measurements at higher energies where higher partial waves contribute. Figure 1(a) shows $\sigma_{\rm el}$ and $\sigma_\eta^{(1)}$ for $a_{\rm s} = \pm 8$ Å: It may be seen that the cross sections for positive and negative scattering lengths deviate from one another substantially above 40 μK and $\sigma_{\rm el}$ and $\sigma_\eta^{(1)}$ start to differ significantly in the same region. Thus, measurements at temperatures high enough to determine the sign of the scattering length should take into account the difference between $\sigma_{\rm el}$ and $\sigma_\eta^{(1)}$.

The remaining panels of Fig. 1 show analogous results for other values of $|a_{\rm s}|$, in order to illustrate the range of possible behavior for other systems. These are chosen to be multiples of the mean scattering length $\bar{a}$ [17], which is 19.3 Å for ^{6}Li^{174}Yb. The corresponding energy scale is $\bar{E} = \hbar^2/2\mu\bar{a}^2$, which is 11.2 mK here. It may be seen that, in most cases, $\sigma_{\rm el}$ and $\sigma_\eta^{(1)}$ are reasonably similar at energies up to about 100 μK (about $10^{-2}\bar{E}$); this may be compared with the p-wave barrier height of 2.8 mK. However, the difference between $\sigma_{\rm el}$ and $\sigma_\eta^{(1)}$ begins at much lower energies (near 1 μK) for values of $a_{\rm s}$ near $+2\bar{a}$. This occurs because angular-momentum-insensitive quantum-defect theory (AQDT) predicts a p-wave shape resonance close to zero collision energy when $a_{\rm s} = +2\bar{a}$ [18] for a potential curve that behaves as $-C_6 R^{-6}$ at long range. The resonance-enhanced p-wave scattering introduces interference terms into Eq. (3) even at very low energy.

AQDT predicts that, in the absence of Feshbach resonances, low-energy elastic scattering for all partial waves can be described by a single parameter which is linked uniquely to the ratio $a_{\rm s}/\bar{a}$. Hence, any two systems which have the same $a_{\rm s}/\bar{a}$ should have identical scattering properties in suitably reduced units within a certain energy range around threshold. Full details are given by Gao [19,20].

The relationship between scattering in different partial waves is conveniently demonstrated by considering the relationship between the s-wave scattering length and the equivalent quantities for higher partial waves [20] (which are no longer lengths but volumes or hypervolumes). For example, the p-wave scattering volume $a_{\rm p}$ is predicted by AQDT to be

$$\frac{a_{\rm p}}{\bar{a}_{\rm p}} = -2\left[1 + \frac{1}{a_{\rm s}/\bar{a} - 2}\right], \tag{4}$$

where $\bar{a}_{\rm p}$ is the mean p-wave scattering volume [20]. Figure 2(a) shows $a_{\rm s}$ and $a_{\rm p}$ for LiYb, from quantum scattering calculations on the realistic potential curves described above, as the potential scaling factor λ is adjusted between 0.8 and 1.2. Figure 2(b) shows $a_{\rm p}$ as a function of $a_{\rm s}$ over the same range of λ. It may be seen that $a_{\rm p}$ is indeed a nearly single-valued function of $a_{\rm s}$ as predicted by Eq. (4).

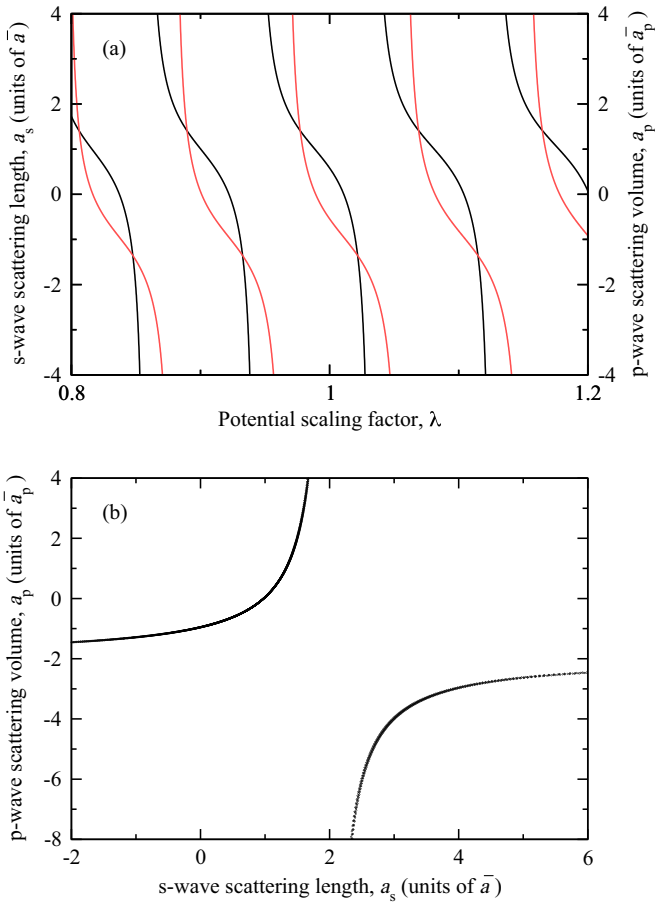

FIG. 2. (Color online) (a) s-wave (black, left scale) and p-wave (red, gray, right scale) scattering lengths and volumes across a wide range of the potential scaling factor λ; (b) a_p as a function of a_s, showing that the different segments of the line in (a) lie on top of one another.

To test the extent of the universal relationship, we have carried out calculations of σ_{el} and $\sigma_\eta^{(1)}$ for RbYb and LiYb for potentials scaled to give identical values of $a_s/\bar{a}$. The results in reduced units are compared for the case of $a_s = 1.05\bar{a}$ in Fig. 3. According to AQDT, values of a_s slightly greater than $\bar{a}$ produce a d-wave shape resonance at low energy, and this appears as a prominent feature for both species in Fig. 3. It may be seen that deviations between σ_{el} and $\sigma_\eta^{(1)}$ are again significant at collision energies above about $10^{-2}\bar{E}$. However, apart from small differences in resonance positions due to the effects of potential terms other than $-C_6R^{-6}$, the results in reduced units are remarkably similar for LiYb and RbYb up to energies around $400\bar{E}$, which is about 4 K for LiYb and 100 mK for RbYb. Similar agreement was obtained for other values of the scattering length. The calculations on full potential curves may also be compared with the results of pure AQDT [19,21], shown in black in Fig. 3.

The universality shown in Fig. 3 allows us to discuss RbYb in terms of the LiYb results shown in Fig. 1, with appropriate scaling of energies and cross sections. The scattering lengths for RbYb vary substantially with Rb and Yb isotopes [9,10,13,22–24]. For ^{87}RbYb, they range from a very small value for ^{87}Rb^{170}Yb to a very large value for ^{87}Rb^{174}Yb, but there are no Yb isotopes that have a_s values near $\bar{a}$.

Figure 4 shows $\sigma_\eta^{(1)}$ for RbYb as a function of the fractional part $\{v_D\}$ of the quantum number at dissociation v_D and the energy in reduced units. Different values of v_D were obtained by scaling the potential of Ref. [13] as described above for LiYb but could equivalently have been achieved by scaling the reduced mass. The s-wave scattering length is related to v_D by

$$a_s = \bar{a}\left[1 - \tan\left(v_D + \frac{1}{2}\right)\pi\right]. \quad (5)$$

It thus has a pole whenever v_D is integer and is large and positive when $\{v_D\}$ is small. Figure 4 thus shows large peaks when $\{v_D\}$ is 0 or 1 and a trough when $\{v_D\} = \frac{3}{4}$ so that $a_s = 0$. In addition, there are strong features due to shape resonances, which sharpen and eventually become invisible as the energy decreases. The ridge that points towards $\{v_D\} = \frac{1}{4}$, $a_s = 2\bar{a}$ at low energy is due to a p-wave resonance, whereas the ones that point towards $\{v_D\} = \frac{1}{2}$, $a_s = \bar{a}$ and $\{v_D\} = \frac{3}{4}$, $a_s = 0$ are due to d-wave and f-wave resonances, respectively. A series of ridges due to shape resonances with higher partial waves may also be seen at higher energies and can be followed up to at least $L = 9$. Their positions closely follow the prediction of AQDT, which is that, at zero energy, resonances with $L \geqslant 4$ occur at the same location as those with $L - 4$. Figure 4 would

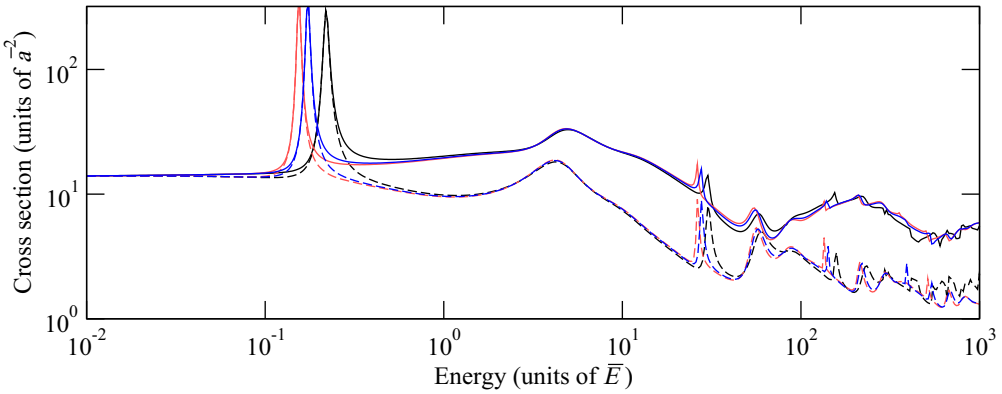

FIG. 3. (Color online) Comparison of σ_{el} (solid lines) and $\sigma_\eta^{(1)}$ (dashed lines) in reduced units with a scattering length of $a_s = 1.05\bar{a}$ for LiYb (red, light gray) and RbYb (blue, dark gray) (mostly indistinguishable except near resonances), compared with analytic AQDT (black) results. The length and energy scaling factors $\bar{a}$ and $\bar{E}$ are 19.3 Å and 11.2 mK for LiYb and 39.6 Å and 270 μK for RbYb.

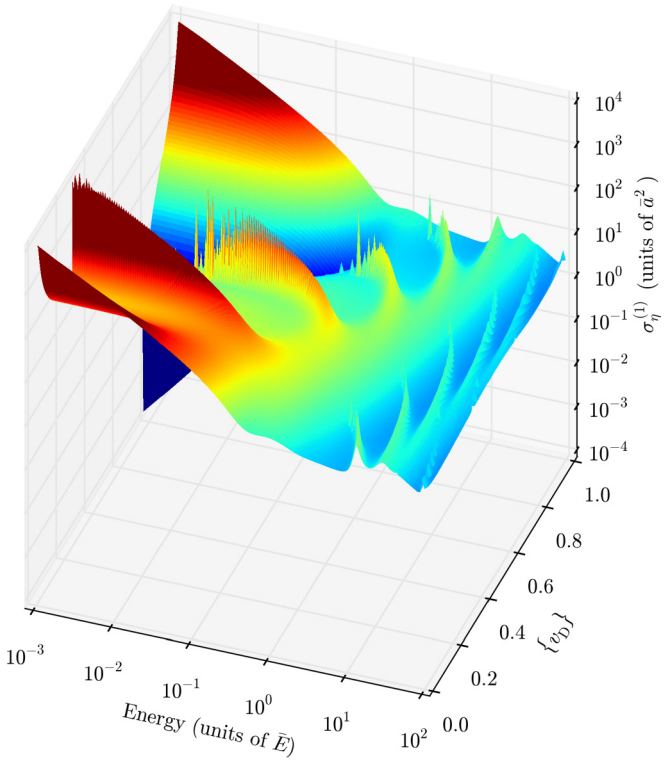

FIG. 4. (Color online) The cross section $\sigma_\eta^{(1)}$ for RbYb as a function of the fractional part $\{v_D\}$ of the quantum number at dissociation and the energy in reduced units. The energy scaling factor $\bar{E}$ is 270 μK for RbYb. The spikes visible at the left-hand end of some narrow ridges are artifacts of the finite grid used for plotting.

look very similar for any other single-channel system with a potential of the form $-C_6R^{-6}$ at long range.

The situation is somewhat more complicated for pairs of alkali-metal atoms and other systems with extensive Feshbach resonances. The overall magnitude of the differences between σ_{el} and $\sigma_\eta^{(1)}$ is likely to be similar in such systems. AQDT still applies usefully to the *background* scattering (away from Feshbach resonances), and in such regions the universal behavior of σ_{el} and $\sigma_\eta^{(1)}$ will still apply, at least at relatively low energies. However, understanding the detailed behavior, including resonant effects, requires coupled-channel calculations using accurate potential curves.

Figure 5 compares calculations on RbCs at various magnetic fields B, using the interaction potential of Ref. [25]. In a magnetic field, $\sigma_\eta^{(1)}$ is no longer given by Eq. (3), but it can still be calculated simply from S-matrix elements [26]. At $B =$ 500 G, the system is in a nonresonant region, and the scattering length is close to its background value, $a_s = a_{bg} \approx 350$ Å $\approx 7.5\bar{a}$; $B = 313.82$ G is in a region with numerous overlapping resonances but where the scattering length is coincidentally close to the background scattering length; and $B = 355$ G is near a resonance but at a point where the scattering length is small, $a_s = 12$ Å. Full coupled-channel calculations on pairs of alkali-metal atoms in a magnetic field become prohibitively expensive for large basis sets, so the coupled-channel results are truncated at $L_{max} = 5$. AQDT results for a single channel with the background scattering length are also shown in Fig. 5. In the nonresonant case, AQDT again gives excellent results for both σ_{el} and $\sigma_\eta^{(1)}$, similar to that seen for the single-channel case with $a_s = 7.5\bar{a}$ in Fig. 1(d). In the resonant case with the same scattering length, the results are again similar, except for a resonant feature that, in this case, occurs near $2\bar{E}$; here $\sigma_\eta^{(1)}$ shows a characteristic peak and trough because the interference terms in Eq. (3) pass through both positive and negative values as one of the phases changes rapidly by π. Even when the scattering length is resonantly shifted from its background value, so that the limitingly low-energy scattering is different, the cross sections rapidly approach the universal form from the background channel once a few partial waves contribute.

III. SUMMARY AND CONCLUSIONS

The cross section that controls thermalization of gas mixtures is the transport cross section $\sigma_\eta^{(1)}$ and not the elastic cross section σ_{el}. We have investigated the behavior of both these cross sections for the prototype systems LiYb and RbYb,

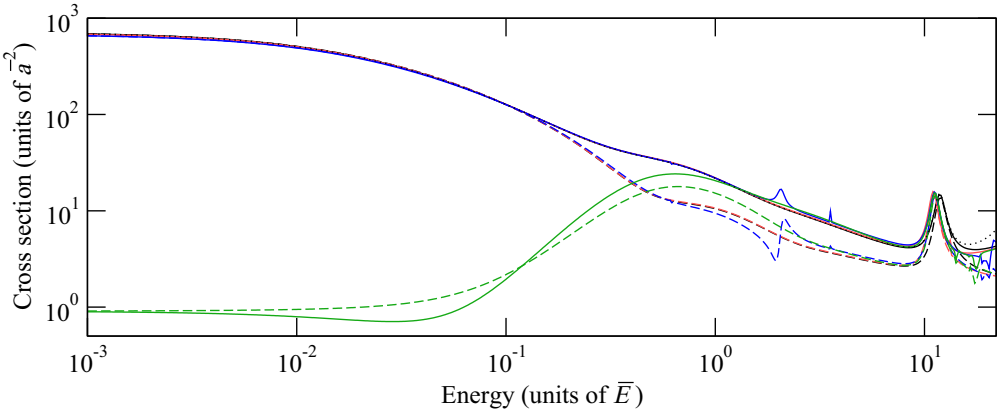

FIG. 5. (Color online) Coupled-channel calculations of σ_{el} (solid lines) and $\sigma_\eta^{(1)}$ (dashed lines) for RbCs at various magnetic fields: 500 G (nonresonant, red, light gray); 313.82 G (resonant but $a_s = a_{bg}$, blue, dark gray); 355 G (resonant, with $a_s \neq a_{bg}$, green, lower gray lines), compared with single-channel AQDT (black). The coupled-channel calculations are truncated at $L_{max} = 5$. Fully converged AQDT results for σ_{el} are shown as a black dotted line and are indistinguishable from the $L_{max} = 5$ results except at the highest energies. The length and energy scaling factors $\bar{a}$ and $\bar{E}$ are 46 Å and 218 μK for RbCs.

which are of current experimental interest. The two cross sections are identical in the pure s-wave regime but differ at higher energies when additional partial waves contribute to the scattering. Measurements at such energies are often desirable to determine the *sign* of the scattering length as well as its magnitude. At energies high enough for the sign to make a difference, $\sigma_\eta^{(1)}$ and $\sigma_{\rm el}$ are significantly different. The differences can appear at very low energies when the s-wave scattering length is close to $+2\bar{a}$, since then there is a p-wave shape resonance close to threshold.

For more complex cases, such as pairs of alkali-metal atoms, resonances may have a large effect on s-wave scattering, but the cross sections nevertheless approach the universal form based on the background scattering length once several partial waves contribute to the scattering. In this regime, the distinction between $\sigma_{\rm el}$ and $\sigma_\eta^{(1)}$ is again significant.

ACKNOWLEDGMENTS

The authors are grateful to Daniel Brue for discussions about the alkali-Yb systems and acknowledge support from the Engineering and Physical Sciences Research Council under Grant No. EP/I012044/1 and from EOARD under Grant No. FA8655-10-1-3033.

[1] R. deCarvalho, J. M. Doyle, B. Friedrich, T. Guillet, J. Kim, D. Patterson, and J. D. Weinstein, Eur. Phys. J. D **7**, 289 (1999).
[2] G. Delannoy, S. G. Murdoch, V. Boyer, V. Josse, P. Bouyer, and A. Aspect, Phys. Rev. A **63**, 051602 (2001).
[3] S. Tokunaga, W. Skomorowski, R. Moszynski, P. S. Żuchowski, J. M. Hutson, E. A. Hinds, and M. R. Tarbutt, Eur. Phys. J. D **65**, 141 (2011).
[4] G. C. Maitland, M. Rigby, E. B. Smith, and W. A. Wakeham, *Intermolecular Forces* (Oxford University Press, Oxford, 1981).
[5] W.-K. Liu, F. R. McCourt, D. E. Fitz, and D. J. Kouri, J. Chem. Phys. **71**, 415 (1979).
[6] M. Anderlini and D. Guéry-Odelin, Phys. Rev. A **73**, 032706 (2006).
[7] V. V. Ivanov, A. Y. Khramov, A. H. Hansen, W. H. Dowd, F. Münchow, A. O. Jamison, and S. Gupta, Phys. Rev. Lett. **106**, 153201 (2011).
[8] H. Hara, Y. Takasu, Y. Yamaoka, J. M. Doyle, and Y. Takahashi, Phys. Rev. Lett. **106**, 205304 (2011).
[9] F. Baumer, Ph.D. thesis, Heinrich-Heine-Universität, 2010.
[10] F. Baumer, F. Münchow, A. Görlitz, S. E. Maxwell, P. S. Julienne, and E. Tiesinga, Phys. Rev. A **83**, 040702 (2011).
[11] P. S. Żuchowski, J. Aldegunde, and J. M. Hutson, Phys. Rev. Lett. **105**, 153201 (2010).
[12] D. A. Brue and J. M. Hutson, Phys. Rev. Lett. **108**, 043201 (2012).
[13] D. A. Brue and J. M. Hutson, Phys. Rev. A **87**, 052709 (2013).
[14] J. M. Hutson and S. Green, MOLSCAT computer program version 14, distributed by Collaborative Computational Project No. 6 of the Engineering and Physical Sciences Research Council (Daresbury, U.K., 1994).
[15] J. M. Hutson and S. Green, SBE computer program, distributed by Collaborative Computational Project No. 6 of the Engineering and Physical Sciences Research Council (Daresbury, U.K., 1982).
[16] P. Zhang, H. R. Sadeghpour, and A. Dalgarno, J. Chem. Phys. **133**, 044306 (2010).
[17] G. F. Gribakin and V. V. Flambaum, Phys. Rev. A **48**, 546 (1993).
[18] B. Gao, Phys. Rev. A **62**, 050702 (2000).
[19] B. Gao, Phys. Rev. A **64**, 010701 (2001).
[20] B. Gao, Phys. Rev. A **80**, 012702 (2009).
[21] B. Gao, Routines to calculate the AQDT parameters for an attractive $1/r^6$ potential, Version 2 (University of Toledo, Ohio, 2003).
[22] F. Münchow, C. Bruni, M. Madalinski, and A. Görlitz, Phys. Chem. Chem. Phys. **13**, 18734 (2011).
[23] F. Münchow, Ph.D. thesis, Heinrich-Heine-Universität, 2012.
[24] M. Borkowski, P. S. Żuchowski, R. Ciuryło, P. S. Julienne, D. Kedziera, L. Mentel, P. Tecmer, F. Münchow, C. Bruni, and A. Görlitz, Phys. Rev. A **88**, 052708 (2013).
[25] T. Takekoshi, M. Debatin, R. Rameshan, F. Ferlaino, R. Grimm, H.-C. Nägerl, C. R. Le Sueur, J. M. Hutson, P. S. Julienne, S. Kotochigova, and E. Tiemann, Phys. Rev. A **85**, 032506 (2012).
[26] R. V. Krems and A. Dalgarno, in *Fundamental World of Quantum Chemistry*, edited by E. J. Brändas and E. S. Kryachko, Vol. 3 (Kluwer Academic, Dordrecht, 2004), pp. 273–294.